JOURNAL OF GUIDANCE, CONTROL, AND DYNAMICS
Vol. 26, No. 1, January–February 2003

Detecting Global Positioning Satellite Orbit Errors Using Short-Baseline Carrier-Phase Measurements

Boris Pervan* and Fang-Cheng Chan†
Illinois Institute of Technology, Chicago, Illinois 60616-3793

A system to detect orbit errors affecting differential global positioning system integrity is described. The method is based on the use of carrier-phase ranging measurements made by two or more ground-based reference receivers separated by short baselines. A dual-frequency, geometry-free widelane approach is used to resolve cycle ambiguities present in the carrier-phase measurements. The performance of the proposed integrity monitor is evaluated relative to existing integrity requirements for aircraft landing navigation applications. The results show that real-time protection is achievable against all types of ephemeris errors that can influence aircraft precision approach and landing navigation.

Introduction

ALTHOUGH initially developed to support military applications, the global positioning system (GPS) has quickly grown into an important and versatile civil navigation utility. The differential GPS (DGPS) technique, in particular, has provided improvements in positioning accuracy sufficient for many demanding applications, including aircraft navigation during precision approach and landing phases of flight. However, for such difficult applications, high accuracy is generally not sufficient. The navigation system must also provide a means to ensure its own integrity by reliably detecting navigation system failures or anomalies. In this work, detailed consideration is given to the real-time detection of a specific type of navigation failure: incorrect knowledge of a GPS satellite orbit.

Each GPS satellite broadcasts orbit ephemerides so users can compute satellite locations at any time of interest. The satellite locations, together with ranging measurements also obtained from the satellite signals, are used to compute user position. An error in knowledge of satellite position will, therefore, cause a resulting error in the computed user position. Nominally, these errors are negligibly small for DGPS users, but integrity considerations for aircraft precision landing navigation dictate that anomalous conditions must be quickly detected. Furthermore, the effects of orbit anomalies differ from those of other navigation failures, for example, GPS receiver failures, in that orbit errors ultimately cause navigation errors that are dependent on the time-varying displacement between the aircraft and ground-based DGPS reference receiver. Therefore, the impact of undetectable orbit errors on navigation must ultimately be assessed separately by each individual aircraft within the DGPS service volume. In this regard, the Federal Aviation Administration (FAA), RTCA, Inc., and the International Civil Aviation Organization (ICAO) are developing specific ephemeris integrity performance standards for DGPS-based aircraft precision landing. The FAA's local-area augmentation system (LAAS) will serve as the baseline DGPS architecture considered in this paper.

Whenever the GPS data broadcast by the satellites do not contain the correct satellite orbit parameters, an ephemeris anomaly is said to exist. Although there may be a variety of potential causes for such anomalies, for example, unscheduled maneuvers, incorrect orbit uploads, and faulted data decoding in the receiver, all ephemeris errors can be categorized into just two classes: type A, where the broadcast ephemeris data are incorrect after a satellite maneuver, and type B, where the broadcast ephemeris data are incorrect, but no satellite maneuvers are involved. These two failure classes fundamentally differ in that type B ephemeris failures are potentially detectable at onset by direct comparison with an earlier, validated ephemeris broadcast, whereas type A failures are not necessarily detectable by such means. However, both type A and type B failures can potentially be detected directly using GPS ranging measurements, provided that the measurements are collected from receivers with a sufficient baseline separation or the time span of the measurement data is significant relative to the orbit period.

The FAA's wide-area augmentation system (WAAS) is a complementary system to LAAS being developed to provide both GPS ranging and ephemeris corrections to aircraft for use during enroute flight, nonprecision approach, and lateral navigation/vertical navigation (LNAV/VNAV) precision approach. When completed, WAAS will consist of approximately 25 ground-based reference receivers widely spaced across the continental United States, which will provide the ability for accurate determination of GPS satellite orbit errors for those users within the coverage area. In contrast, LAAS systems will be sited locally at airports to provide the superior accuracy and integrity performance required for category 1–3 precision approach and landing. For LAAS airports within the WAAS coverage area, ephemeris error can be effectively mitigated by the use of WAAS ephemeris corrections. However, such a solution to ephemeris monitoring is impossible for airports outside the service areas of WAAS (or the equivalent wide-area systems currently being developed in Europe and Asia). For this reason, many of the world's airports will have to rely on LAAS capabilities alone to detect ephemeris errors for precision approach and landing navigation. Furthermore, even within WAAS service areas, it is undesirable from a systems point of view for LAAS to be functionally dependent on the successful operation of another augmentation system. Ideally, the LAAS navigation system should be able to function with or without WAAS so that, in the event of a WAAS failure, all LAAS systems would not also cease to function as a consequence. In this context, an independent local-area solution to the ephemeris monitoring problem is highly desirable.

To date, a relatively small amount of effort has been focused on independent ephemeris monitoring for LAAS. In the LAAS ground facility (LGF) specification,[1] for example, it is required that the consistency of new and old ephemeris messages be verified before a satellite is declared usable for navigation. However, as already noted, such monitoring is insufficient against type A failures because prior ephemeris data (which may be used in the consistency check) is of no use after a satellite maneuver.

A well-known approach to GPS fault detection, which can be effective against many different types of failures, is the receiver autonomous integrity monitor (RAIM) method.[2–4] The RAIM concept is based on the verification of the consistency of redundant satellite

Received 26 March 2002; revision received 10 June 2002; accepted for publication 11 June 2002.

*Assistant Professor, Department of Mechanical, Materials and Aerospace Engineering, Engineering 1 Building, 10 West 32nd Street. Member AIAA.
†Graduate Student, Department of Mechanical, Materials and Aerospace Engineering, Engineering 1 Building, 10 West 32nd Street.

measurements by the GPS user (the aircraft on final approach in this case). However, the time availability of RAIM is limited by the need for redundant satellites with favorable line-of-sight geometries. Furthermore, for aircraft navigation with LAAS, it is a system requirement that space segment failures must be detected and isolated on the ground by the LGF before differential corrections are broadcast. (The aircraft is accountable only for the management of failures in its own navigation avionics.) Therefore, RAIM in the traditional sense is not a viable candidate for LAAS ephemeris monitoring. However, these requirements do not necessarily preclude the execution of RAIM-like algorithms on the ground, as will be discussed.

The most relevant difference of the LGF from other DGPS architectures is the existence of multiple reference receivers on the airport property separated by precisely surveyed short baselines (a few hundred meters in length). The use of multiple reference receivers provides a means for detection and isolation of a failed receiver and also allows for a net reduction in ranging error by averaging ranging measurements for a given satellite across receivers. Spatial separation of the receivers is necessary in this regard to ensure sufficient decorrelation of ground multipath errors so that the averaging process is effective. However, a generally unrecognized additional benefit of this spatial separation is that ephemeris anomalies (both types A and B) can potentially be directly observed. As will be shown in the next section, an ephemeris anomaly will cause an effective differential ranging error between two receivers that increases in proportion with the baseline length between the receivers. For example, an aircraft on final approach will have a displacement from the LGF reference receivers that is generally much larger than the distances between the reference receivers themselves. Therefore, the effect of an ephemeris anomaly for an aircraft on final approach will be proportionately larger than the effect of the same ephemeris error observed across the reference receiver baselines. To compensate for this relative insensitivity caused by the short LGF baselines, the ground-based ephemeris monitor must use measurements with low noise (so that ephemeris anomaly effects can be more clearly observed). A natural source of such measurements in this application is the GPS carrier phase.[5] Using carrier-phase measurements, tight thresholds for ephemeris anomaly detection may be set without incurring high false alarm rates. However, the use of carrier phase for real-time monitoring applications is contingent on the successful and timely resolution of carrier-cycle ambiguities for newly rising satellites.

Whereas the details of the short baseline, carrier-phase monitor architecture will be discussed in the subsequent sections of this paper, we note at the outset that such a monitor can conceivably be implemented in either the position or range domain. In the position-domain method, the baseline vector between reference receivers is recomputed in real-time using current GPS carrier measurements, and the result is compared with the known presurveyed vector. However, because the LGF cannot know what GPS satellites any given aircraft is tracking, it is necessary to repeat the position-domain computation for all practical subsets of satellites in view. The performance of such a position-domain monitor will be comparatively poor because thresholds must be set loose enough to account for the relatively large fault-free position errors associated with satellite subsets. In contrast, in the range-domain method, the difference in ranging measurements across the reference receiver baselines is computed for each individual satellite, and the result is compared to the projection of the presurveyed baseline vector into the satellite line-of-sight directions. Using the range-domain approach, thresholds can be kept tight for individual satellites, and aircraft are able to translate easily the range-domain monitor performance into the position domain for the actual satellite subset being tracked, leading to superior performance. For this reason, the range-domain approach has been standardized by the FAA, RTCA, and ICAO and will be the method used in this work.

In this paper, we describe the effects of orbit anomalies on DGPS systems and introduce a detection method using short-baseline, carrier-phase measurements. The related cycle ambiguity resolution problem is also addressed in detail. In this regard, a dual-frequency ephemeris monitor architecture is proposed to meet the integrity requirements of LAAS and provide real-time warning capability. It is shown that the dual-frequency monitor architecture can fulfill the objective with realizable LGF hardware.

Orbit Error Effects in DGPS

Consider two GPS receivers (a and b) separated by a (3×1) baseline vector $\boldsymbol{x}_{ab}$. GPS L1 band carrier-phase measurements from the two receivers for an arbitrary satellite i can be expressed as

$$\lambda_1 \phi_a^i = r_a^i + c(\delta t_i - \delta t_a) - I_i + T_i + \lambda_1 N_a^i + \nu_\phi^i \tag{1}$$

$$\lambda_1 \phi_b^i = r_b^i + c(\delta t_i - \delta t_b) - I_i + T_i + \lambda_1 N_b^i + \nu_\phi^i \tag{2}$$

where λ_1 is the wavelength of the L1 carrier signal; ϕ_a^i is the carrier-phase measurement for satellite i on receiver a; r_a^i is the range between satellite i and reference receiver a; c is speed of light; δt_i and δt_a are clock biases (relative to GPS system time) for satellite i and receiver a, respectively; I_i is the ionospheric phase advance for satellite i; T_i is the tropospheric delay for satellite i; N_a^i is the unknown integer-cycle ambiguity associated with satellite i and receiver a; and ν_ϕ^i is the measurement error due to receiver noise and multipath. All of these definitions are also applicable to the carrier-phase measurement for satellite i on receiver b by replacing a with b. We assume that $\boldsymbol{x}_{ab}$ is short enough that ionosphere and troposphere ranging errors are the same for the two receivers.

A single-difference carrier-phase measurement can be obtained by subtracting Eq. (2) from Eq. (1):

$$\lambda_1 \Delta\phi_{ab}^i = \Delta r_{ab}^i + c(\delta t_b - \delta t_a) + \lambda_1 \Delta N_{ab}^i + \Delta \nu_\phi^i \tag{3}$$

where $\Delta\phi_{ab}^i \equiv \phi_a^i - \phi_b^i$, $\Delta r_{ab}^i \equiv r_a^i - r_b^i$, and $\Delta N_{ab}^i \equiv N_a^i - N_b^i$.

For baselines much smaller than the distance to the satellite (over 20,000 km), the receiver-to-satellite line-of-sight unit vectors are essentially identical for both receivers; thus, Δr_{ab}^i in Eq. (3) can be expressed as

$$\Delta r_{ab}^i = \boldsymbol{e}_{i,\text{true}}^T \boldsymbol{x}_{ab} = (\boldsymbol{e}_i + \delta\boldsymbol{e}_i)^T \boldsymbol{x}_{ab} = \boldsymbol{e}_i^T \boldsymbol{x}_{ab} + \delta\boldsymbol{e}_i^T \boldsymbol{x}_{ab} \tag{4}$$

where $\boldsymbol{e}_{i,\text{true}}$ is the true line-of sight vector (3×1), $\boldsymbol{e}_i$ is line-of-sight vector computed from the available ephemeris data broadcast by the satellite, and $\delta\boldsymbol{e}_i$ is the vector error in the line of sight. The last term, $\delta\boldsymbol{e}_i^T \boldsymbol{x}_{ab}$, represents the effective differential ranging error due to an error in knowledge of satellite position. We define this differential ranging error for satellite i as

$$\lambda_1 \delta\Delta\phi_i \equiv \delta\boldsymbol{e}_i^T \boldsymbol{x}_{ab} \tag{5}$$

Given a vector error (3×1) in knowledge of satellite position $\delta\boldsymbol{R}_i$, it is shown in Ref. 6 that the resulting line-of-sight unit vector error is

$$\delta\boldsymbol{e}_i = \left(1/r_a^i\right)\left(\boldsymbol{I} - \boldsymbol{e}_i\boldsymbol{e}_i^T\right)\delta\boldsymbol{R}_i \tag{6}$$

Substituting Eq. (6) into Eq. (5), we can express differential ranging error directly as a function of satellite position error ($\delta\boldsymbol{R}_i$) and the baseline vector $\boldsymbol{x}_{ab}$ between the two receivers:

$$\lambda_1 \delta\Delta\phi_i = \left(1/r_a^i\right)\delta\boldsymbol{R}_i^T\left(\boldsymbol{I} - \boldsymbol{e}_i\boldsymbol{e}_i^T\right)\boldsymbol{x}_{ab} \tag{7}$$

To illustrate quantitatively the effect of orbit error, we consider a satellite whose line-of-sight vector is given by an elevation angle θ and an azimuth angle ψ. (Azimuth is defined relative to the direction of the horizontal baseline vector $\boldsymbol{x}_{ab}$.) In local coordinates (where $\hat{\boldsymbol{i}}_1$ is parallel to $\boldsymbol{x}_{ab}$ and $\hat{\boldsymbol{i}}_3$ is vertical) shown in Fig. 1, the line-of-sight vector can be represented as

$$\boldsymbol{e}_i = \cos\theta\cos\psi\hat{\boldsymbol{i}}_1 + \cos\theta\sin\psi\hat{\boldsymbol{i}}_2 + \sin\theta\hat{\boldsymbol{i}}_3 \tag{8}$$

Expressed in this coordinate frame, a baseline vector with length b is $\boldsymbol{x}_{ab} = [b \;\; 0 \;\; 0]^T$. When this baseline vector and Eq. (8) are

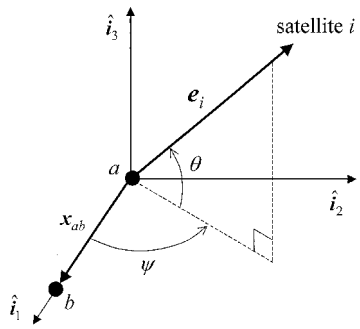

Fig. 1 Baseline and satellite relative geometry.

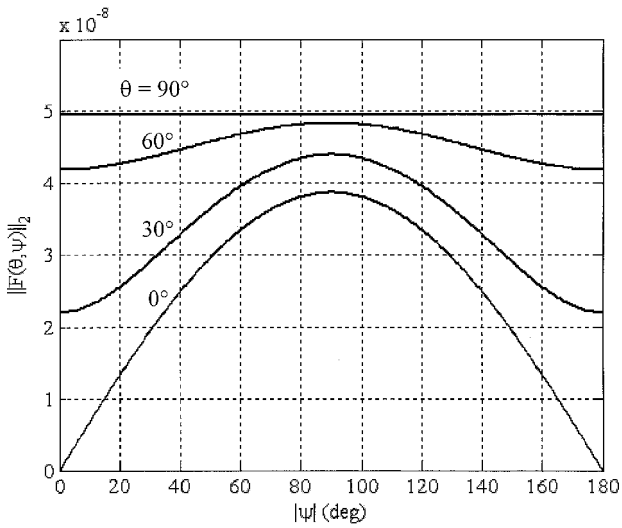

Fig. 2 Worst-case differential ranging error sensitivity.

substituted into Eq. (7), and divided through by length b (scalar), the normalized single differential ranging error becomes

$$\lambda_1 \delta\Delta\phi_i / b = \left(1 / r_a^i\right) \times \left[(1 - \cos^2\theta\cos^2\psi) \quad -\cos^2\theta\sin\psi\cos\psi \quad -\cos\theta\sin\theta\cos\psi\right] \delta\boldsymbol{R}_i \tag{9}$$

Using the law of cosines, the distance r_a^i can be expressed in terms of the satellite elevation angle θ, the Earth's radius r_E, and the radius of satellite orbit r_S:

$$r_a^i = \sqrt{r_S^2 - r_E^2\cos^2\theta} - r_E\sin\theta \tag{10}$$

When Eq. (10) is substituted into Eq. (9), the relation between normalized single differential ranging error and satellite orbit error is

$$\lambda_1 \delta\Delta\phi_i / b = \boldsymbol{F}(\theta,\psi)^T \delta\boldsymbol{R}_i \tag{11}$$

where

$$\boldsymbol{F}(\theta,\psi) = \frac{1}{\sqrt{r_S^2 - r_E^2\cos^2\theta} - r_E\sin\theta} \begin{bmatrix} 1 - \cos^2\theta\cos^2\psi \\ -\cos^2\theta\sin\psi\cos\psi \\ -\cos\theta\sin\theta\cos\psi \end{bmatrix}$$

The upper bound on the differential ranging error (applicable to the worst-case direction for $\delta\boldsymbol{R}_i$) is given by

$$|\lambda_1 \delta\Delta\phi_i / b| \le \|\boldsymbol{F}(\theta,\psi)\|_2 \|\delta\boldsymbol{R}_i\|_2 \tag{12}$$

The vector norm $\|\boldsymbol{F}(\theta,\psi)\|_2$ defines the worst-case sensitivity to an orbit displacement for a satellite with line of sight defined by angles θ and ψ. Figure 2 shows contours of $\|\boldsymbol{F}(\theta,\psi)\|_2$ for $|\psi|$ between 0 and 180 deg and θ equal to 0, 30, 60, and 90 deg.

It is evident from Fig. 2 that only zero-elevation satellites with baseline-relative azimuths of 0 or 180 deg will experience zero effective differential ranging error regardless of orbit error direction or magnitude. In all other cases, a differential ranging error can exist (depending on the orbit error direction), the largest possible magnitudes occurring for high-elevation satellites. Furthermore, it is clear directly from Eq. (7) that only components of satellite position error orthogonal to the satellite line-of-sight direction contribute to the equivalent differential ranging error. The magnitude of differential ranging error is always proportional to the distance between the DGPS reference receiver a and the user receiver b.

LAAS

In this work, we are particularly interested in the impact of orbit errors on DGPS navigation for aircraft precision landing applications. In this regard, a brief review of the relevant navigation requirements is necessary. The DGPS system being developed under the direction of FAA is known as the LAAS. The navigation performance requirements for the system are rated according to a three-tiered structure (category 1–3) corresponding to the levels of approach visibility during bad weather conditions. A category 3-capable facility will support automatic precision landing operation and has the most stringent requirements. In this work, we will focus on category 3 systems.

Figure 3 shows the configuration for an aircraft precision approach/landing and provides graphical definitions of some related terminology: glide path intercept point (GPIP), glide path angle (GA) (nominally 3 deg), and aircraft height H.

The allocation of specific requirements for the navigation system is based on four fundamental parameters.[7,8]

1) *Accuracy* is the measure of the navigation output deviation from truth under fault-free conditions and is often specified in terms of 95% performance.

2) *Integrity* is the ability of a system to provide timely warnings to users when the system should not be used for navigation. Integrity risk is the probability of an undetected navigation error or failure that results in hazardously misleading information onboard the aircraft.

3) *Continuity* is the likelihood that the navigation signal in space supports accuracy and integrity requirements for the duration of intended operation. Continuity risk is the probability of a detected but unscheduled navigation function interruption after an approach has been initiated.

4) *Availability* is the fraction of time the navigation function is usable (as determined by its compliance with the accuracy, integrity, and continuity requirements) before the approach is initiated.

Tables 1 and 2 list the vertical navigation requirements for category 3 LAAS implementations.[9] Because the vertical navigation requirements are more stringent than those for lateral navigation, our focus here will be on meeting the vertical requirements.

Table 1 Vertical accuracy requirements for LAAS category 3

95% vertical accuracy, m	Height H of aircraft above runway, ft
$\le$2.0	$H \le 100$ (30.48 m)
$\le 0.0117 \times H$(ft) + 0.83	100 (30.48 m) $< H \le$ 1290 (393.19 m)
$\le$15.9	$H >$ 1290 (393.19 m)

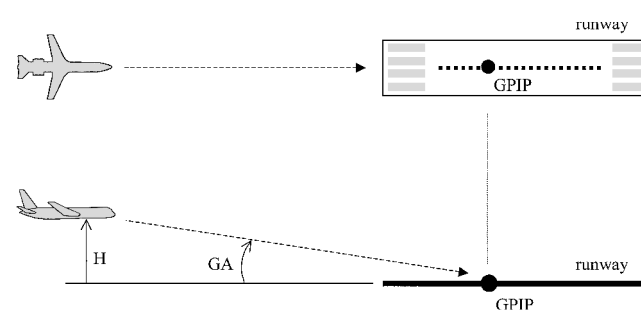

Fig. 3 Aircraft approach configuration.

Table 2 Integrity, continuity, and availability requirements for LAAS category 3

Requirement	Value
Integrity risk	1×10^{-9} per approach
Continuity risk	2×10^{-6}/s (vertical)
Availability	0.99–0.99999

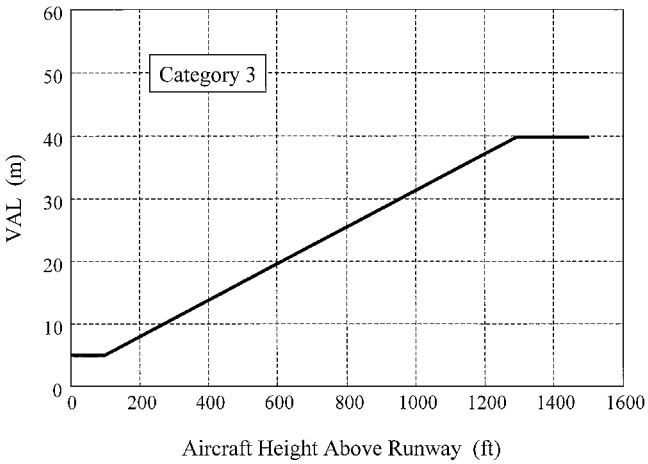

Fig. 4 VAL integrity requirement for precision landing.

In addition to the requirements listed in Tables 1 and 2, a minimum vertical alert limit (VAL) for category 3 LAAS, which is applicable below a height of 100 ft, is defined in Ref. 9 to be $\text{VAL}_{\min} = 5.3$ m. Above a height of 100 ft, VAL is defined as 2.5 times the 95% vertical accuracy requirement.[9] The VAL represents an integrity containment surface in the sense that the probability of an undetected vertical position error exceeding the VAL must be less than 10^{-9} (the integrity risk requirement in Table 2). This integrity requirement applies for both fault-free and faulted (for example, orbit anomaly) cases. Figure 4 is a plot of VAL vs aircraft height for category 3. (For consistency with the LAAS specifications in Table 2, height is expressed in feet and VAL is expressed in meters.)

Integrity monitoring performance in LAAS is quantified through the computation of position error bounds associated with the maximum permissible integrity risk probability. These vertical bounds are known as the vertical protection levels (VPL) and are computed at the aircraft during an approach to verify that VPL < VAL. VPL values are generated under multiple operational hypotheses (fault-free, failed reference receiver, and ephemeris failure) using current satellite geometry information, known nominal measurement error statistics, and additional parameters (derived from ground-based integrity monitor performance) that are broadcast to the aircraft from the ground. More detail on VPL will be given shortly.

Orbit Monitor Concept

The LAAS system uses smoothed GPS pseudorange (code-phase) measurements for positioning. Although these are less precise than carrier-phase measurements, the precision is sufficient to meet navigation accuracy requirements for aircraft landing when high-quality antennas and receivers are used. The use of pseudorange measurements for positioning offers an additional operational advantage over carrier measurements in that unknown cycle ambiguities (present in the carrier measurements only) need not be resolved by the aircraft. It is important to understand that the differential ranging error caused by an ephemeris anomaly is a geometric effect, which is the same for both code and carrier measurements. However, for a given baseline length, the differential ranging error caused by an ephemeris anomaly is more easily observed (by a monitor on the ground, for example) using carrier measurements because other nominal ranging errors (multipath and receiver thermal noise), which are also present in the measurements, are much smaller. In this section, we mathematically relate the magnitude of the carrier-phase residuals measured across LAAS reference receiver baselines to the magnitude of navigation errors suffered by an incoming aircraft. We then introduce a detection threshold on the carrier-phase residual to ensure an acceptably low monitor false alarm rate (consistent with LAAS continuity requirements) and define a resulting operational bound on aircraft position error such that LAAS integrity requirements are identically satisfied.

When Eq. (11) is used and the effect of other nominal measurement errors is included, the pseudorange single difference between reference station and aircraft ranging error for a satellite with an ephemeris failure can be written directly:

$$\delta\Delta\rho_f = \left(\boldsymbol{F}_f^T \delta \boldsymbol{R}_f\right) x + \Delta\nu_\rho^f \tag{13}$$

where the sub/superscript f is the index of the failed satellite, x is a scalar displacement between the aircraft antenna and the geometric centroid of the reference antennas, and $\Delta\nu_\rho^f$ is the nominal single-difference measurement error for the failed satellite. Recall that $\boldsymbol{F}_f$ is a function of the elevation and azimuth (relative to the direction of the displacement x) of satellite f. We assume for the present that the aircraft is in the local horizontal plane. The effect of the nominal 3-deg glide path angle will be addressed shortly.

Because, the ephemeris messages for each satellite are created and broadcast independently, and ephemeris anomalies are low probability events (based on GPS system performance to date[10]), the likelihood of multiple, simultaneous ephemeris failures is assumed to be negligible. Therefore, the maximum number of satellites with ephemeris failures at any time is assumed to be one. For the other healthy satellites, the nominal pseudorange single differential ranging error is then

$$\delta\Delta\rho_i = \Delta\nu_\rho^i \tag{14}$$

The nominal pseudorange error ($\Delta\nu_\rho^i$) for each satellite is assumed to be independent and identically normally distributed with zero mean and standard deviation $\sigma_{\Delta\rho}$. For carrier-phase measurements, the same assumptions apply except that the analogous standard deviation $\sigma_{\Delta\phi}$ is much smaller.

Assume now that we have available a single-difference carrier-phase measurement ($\Delta\phi_f$), with its cycle ambiguity known and removed, from two ground-based reference receivers aligned with the approach path direction and separated by baseline length b. (Resolution of the cycle ambiguity will be discussed shortly.) In this case, using Eq. (11) with nominal error term included, we have for the failed satellite:

$$\left(\lambda_1 \delta\Delta\phi_f - \Delta\nu_\phi^f\right)/b = \boldsymbol{F}_f^T \delta \boldsymbol{R}_f$$

Substituting this expression into Eq. (13), the pseudorange single difference ranging error can be expressed as

$$\delta\Delta\rho_f = \left[\left(\lambda_1 \delta\Delta\phi_f - \Delta\nu_\phi^f\right)/b\right] x + \Delta\nu_\rho^f \tag{15}$$

To determine the aircraft position error for given satellite geometry with n satellites ($n \geq 4$), we first stack the available single-difference pseudorange measurements:

$$\begin{bmatrix} \Delta\rho_1 \\ \vdots \\ \Delta\rho_f \\ \vdots \\ \Delta\rho_n \end{bmatrix} = \underbrace{\begin{bmatrix} -\boldsymbol{e}_1^T & 1 \\ \vdots & \vdots \\ -\boldsymbol{e}_f^T & 1 \\ \vdots & \vdots \\ -\boldsymbol{e}_n^T & 1 \end{bmatrix}}_{\boldsymbol{G}} \begin{bmatrix} x_{a/c} \\ y_{a/c} \\ z_{a/c} \\ cb \end{bmatrix} + \begin{bmatrix} \delta\Delta\rho_1 \\ \vdots \\ \delta\Delta\rho_f \\ \vdots \\ \delta\Delta\rho_n \end{bmatrix}$$

The least-squares estimate error is then

$$\begin{bmatrix} \delta\hat{x}_{a/c} \\ \delta\hat{y}_{a/c} \\ \delta\hat{z}_{a/c} \\ c\delta\hat{b} \end{bmatrix} = \underbrace{\begin{bmatrix} s_{11} & s_{12} & \cdots & s_{1n} \\ s_{21} & s_{22} & \cdots & s_{2n} \\ \vdots & \vdots & \ddots & \vdots \\ s_{n1} & s_{n2} & \cdots & s_{nn} \end{bmatrix}}_{\boldsymbol{S}} \begin{bmatrix} \delta\Delta\rho_1 \\ \vdots \\ \delta\Delta\rho_f \\ \vdots \\ \delta\Delta\rho_n \end{bmatrix}$$

where $\boldsymbol{S} \equiv (\boldsymbol{G}^T\boldsymbol{G})^{-1}\boldsymbol{G}^T$. The vertical position error, of particular interest for the precision landing application, is

$$\delta\hat{z}_{a/c} = s_{31}\delta\Delta\rho_1 + s_{32}\delta\Delta\rho_2 + \cdots + s_{3f}\delta\Delta\rho_f + \cdots + s_{3n}\delta\Delta\rho_n \tag{16}$$

When Eqs. (14) and (15) are substituted into Eq. (16),

$$\delta\hat{z}_{a/c} = s_{3f}\left[\left(\lambda_1\delta\Delta\phi_f - \Delta v_\phi^f\right)\frac{x}{b}\right] + s_{3f}\Delta v_\rho^f + \sum_{\substack{i=1\\ i\neq f}}^{n} s_{3i}\Delta v_\rho^i$$

$$= s_{3f}\frac{x}{b}\lambda_1\delta\Delta\phi_f - s_{3f}\frac{x}{b}\Delta v_\phi^f + \sum_{i=1}^{n} s_{3i}\Delta v_\rho^i \tag{17}$$

To limit the position error resulting from an ephemeris anomaly, there is a threshold T_s on the test statistic $\lambda_1\delta\Delta\phi_f$ (which is measurable) such that the false alarm probability is not greater than a certain predetermined value P_{fa}, which is derived from the continuity requirement. The basic concept is that if $|\lambda_1\delta\Delta\phi_i|$ exceeds T_s for a given satellite i, then an orbit error is detected for the satellite. A probability multiplier K_{ffde} associated with the value of P_{fa} is defined so that

$$T_s \equiv K_{\text{ffde}}\sigma_{\Delta\phi} \tag{18}$$

where $\sigma_{\Delta\phi}$ is the standard deviation of the nominal differential carrier-phase measurement error. With this detection algorithm in place on the ground, it is always true that

$$|\lambda_1\delta\Delta\phi_f| < K_{\text{ffde}}\sigma_{\Delta\phi} \tag{19}$$

Assuming an ephemeris failure occurs on the worst-case satellite, an inequality relation for vertical position error can then be obtained using Eqs. (17) and (19):

$$|\delta z_{a/c}| \le \|\boldsymbol{s}_{3,:}\|_\infty (x/b) K_{\text{ffde}}\sigma_{\Delta\phi} + |A| \tag{20}$$

where $\|\boldsymbol{s}_{3,:}\|_\infty$ is the absolute value of the largest element of $\boldsymbol{s}_{3,:}$ (the infinity norm) and

$$A \equiv \|\boldsymbol{s}_{3,:}\|_\infty \frac{x}{b}\Delta v_\phi^f + \sum_{i=1}^{n} s_{3i}\Delta v_\rho^i \tag{21}$$

Note that the value of A is a function of random code and carrier nominal measurement errors. Invoking our assumption of independent and identically normally distributed measurement errors, the standard deviation of A is

$$\sigma_A = \sqrt{\|\boldsymbol{s}_{3,:}\|_\infty^2 (x^2/b^2)\sigma_{\Delta\phi}^2 + \|\boldsymbol{s}_{3,:}\|_2^2\sigma_{\Delta\rho}^2} \tag{22}$$

We now proceed to define the VPL under the ephemeris failure hypothesis (VPL_e) based on a required probability of missed detection P_{mde}, which is derived from the integrity requirement. Introducing a second probability multiplier K_{mde} associated with P_{mde}, the protection level can be defined using Eqs. (20) and (22) as

$$\|\boldsymbol{s}_{3,:}\|_\infty K_{\text{ffde}}(x/b)\sigma_{\Delta\phi} + K_{\text{mde}}\sqrt{\|\boldsymbol{s}_{3,:}\|_\infty^2 (x^2/b^2)\sigma_{\Delta\phi}^2 + \|\boldsymbol{s}_{3,:}\|_2^2\sigma_{\Delta\rho}^2} \tag{23}$$

The protection level can be written in a more compact form that is slightly more conservative by noting that

$$\sqrt{\|\boldsymbol{s}_{3,:}\|_\infty^2 (x^2/b^2)\sigma_{\Delta\phi}^2 + \|\boldsymbol{s}_{3,:}\|_2^2\sigma_{\Delta\rho}^2} \le \|\boldsymbol{s}_{3,:}\|_\infty (x/b)\sigma_{\Delta\phi} + \|\boldsymbol{s}_{3,:}\|_2\sigma_{\Delta\rho} \tag{24}$$

In this case, Eq. (23) can be simplified to obtain a standard equation for VPL_e [applicable here to the assumed case of independent and identically distributed (IID) nominal error] which has been proposed for inclusion in the revised version of the LAAS airborne requirements,[11]

$$\text{VPL}_\text{e} \equiv p\|\boldsymbol{s}_{3,:}\|_\infty x + K_{\text{mde}}\|\boldsymbol{s}_{3,:}\|_2\sigma_{\Delta\rho} \tag{25}$$

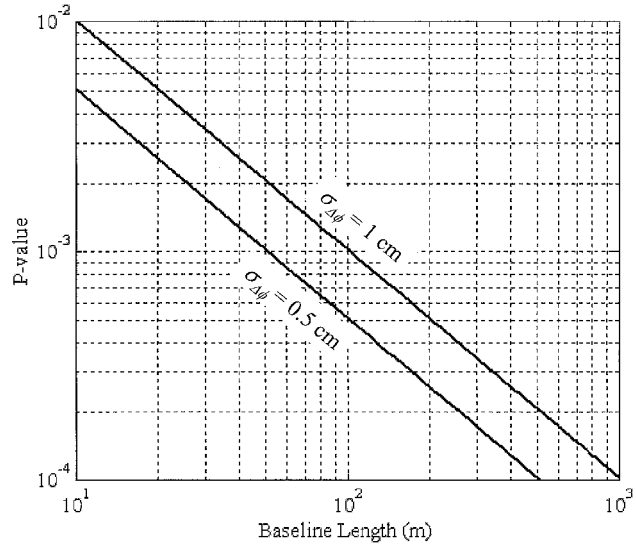

Fig. 5 *P*-value vs baseline length.

where for the proposed carrier-phase monitor

$$p = (K_{\text{ffde}} + K_{\text{mde}})(\sigma_{\Delta\phi}/b) \tag{26}$$

The parameter p, known as the ephemeris decorrelation parameter, can be interpreted as an angle (in radians) defined by the ratio of the minimum detectable ephemeris error (MDE) and the distance to the given satellite r: $p = \text{MDE}/r$. Note that p may also vary by satellite depending on the ground ephemeris monitor implementation, and so the LGF must broadcast separate p values to the aircraft for each satellite. Because it is desired that $\text{VPL}_\text{e} < \text{VAL}$, it is clear from Eq. (25) that performance improves as p is made smaller. For given false alarm and missed detection probabilities, this may be achieved by either decreasing measurement error $\sigma_{\Delta\phi}$ or increasing baseline length b.

A preliminary requirement for the probability of missed detection of satellite failures (based on the integrity risk requirements in Table 2 and verifiable satellite failure prior probabilities) is derived in Ref. 12 to be $P_{\text{mde}} = 5 \times 10^{-7}$. ($K_{\text{mde}} \approx 5.0$ for a standard normal distribution.) Assuming further a false alarm probability (consistent with continuity requirements in Table 2) of $P_{\text{ffde}} = 10^{-7}$ ($K_{\text{ffde}} \approx 5.3$), the value of the parameter p is plotted in Fig. 5 as a function of baseline length for two representative values of $\sigma_{\Delta\phi}$ (0.5 and 1 cm). Although the p value is the only ground monitor performance parameter directly relevant to VPL_e, the results in Fig. 5 can be also easily interpreted in terms of MDE by multiplying p by the distance to the satellite. For example, using a baseline length of 750 m and $\sigma_{\Delta\phi} = 1$ cm, MDE ranges between 3650 m for low-elevation satellites (which are farther away from the receivers) and MDE = 2770 m for high-elevation satellites (which are closer to the receivers).

It is also clear from Eq. (25) that the protection level is a strong function of geometry via the vector norms of $\boldsymbol{s}_{3,:}$. It is entirely possible that, even for small values of p, a given satellite geometry can be sufficiently poor that $\text{VPL}_\text{e} > \text{VAL}$. In such a case, navigation is said to be unavailable. However, it is also true that given a weak satellite geometry, positioning performance will also be poor (due to nominal ranging errors) regardless of whether or not an ephemeris anomaly exists. For this reason, the LAAS architecture also places limits on the worst-case satellite geometries that can be used under normal conditions. Specifically, for all LAAS approaches, the aircraft computes a vertical protection level under the fault-free hypothesis (H0) (Ref. 9). For the IID error case under consideration, satellite geometries are always checked to ensure that

$$\text{VPL}_{\text{H0}} \equiv K_{\text{ff\_md}}\|\boldsymbol{s}_{3,:}\|_2\sigma_{\Delta\rho} < \text{VAL} \tag{27}$$

where the probability multiplier $K_{\text{ff\_md}} \approx 6.6$ (Ref. 9) corresponds to the maximum permissible integrity risk ($<10^{-9}$). To ensure integrity during the entire aircraft approach, the value of VPL_{H0} must not be

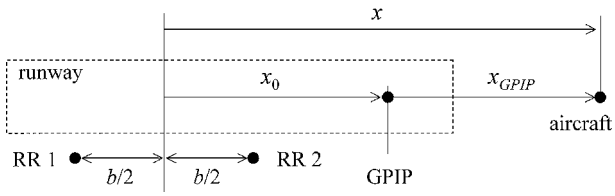

Fig. 6 Baseline-runway configuration.

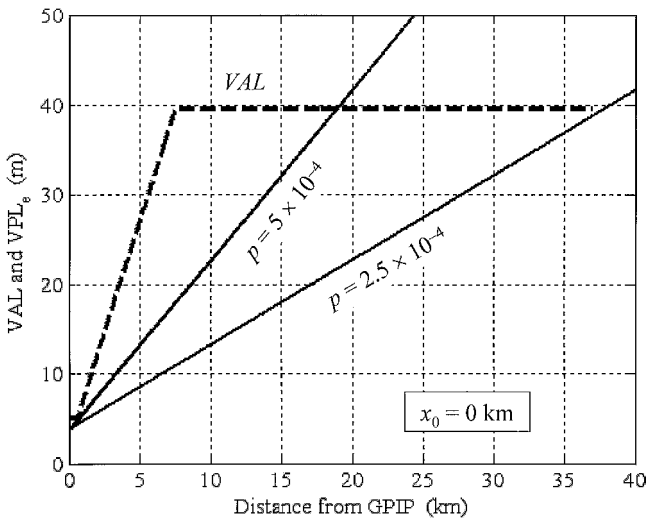

Fig. 7 VPL_e bound vs distance, $x_0 = 0$.

larger than VAL at any time during the approach. When the most stringent constraint, VAL_{min}, which occurs at a height of 100 ft, is considered, the maximum permissible value of $\|s_{3,:}\|_2$ becomes

$$\|s_{3,:}\|_2 \leq \frac{VAL_{min}}{K_{ff\_md}\sigma_{\Delta\rho}} \tag{28}$$

Substituting Eq. (28) into Eqs. (25) and (26), and exploiting that $\|s_{3,:}\|_2 \geq \|s_{3,:}\|_\infty$, we may write

$$VPL_e \leq VAL_{min}\left[\frac{p}{K_{ff\_md}\sigma_{\Delta\rho}}x + \frac{K_{mde}}{K_{ff\_md}}\right] \tag{29}$$

To quantify the upper bound on VPL_e expressed on the right-hand side of inequality (24), we assume $\sigma_{\Delta\rho} = 20$ cm. This is a reasonably conservative assumption in the sense that $\sigma_{\Delta\rho}$, which includes both ground and aircraft ranging error contributions, is likely to be larger in actual LAAS operations.

In Fig. 6, we decompose x into the sum of two displacements: x_0, the distance from GPIP to the geometric centroid of the LGF reference receivers, and x_{GPIP}, the horizontal distance from GPIP to the aircraft. Figure 7 shows the upper bound on VPL_e as a function of the aircraft distance to touchdown x_{GPIP} obtained using relation (29) for $x_0 = 0$ and values of p equal to 5×10^{-4} and 2.5×10^{-4}. As can be inferred from Fig. 5, the selected p values correspond to baseline lengths of approximately 200 and 400 m, respectively, when $\sigma_{\Delta\phi} = 1$ cm. Comparing the VPL_e bounds with the VAL (also shown in Fig. 7), it is evident that a 200-m baseline is sufficient to ensure that $VPL_e < VAL$ in the near field, that is, near the runway. However, at longer distances, the VAL levels at a constant value of approximately 40 m, so that upper-bound VPL_e begins to exceed VAL at a distance of approximately 18 km. When the 400-m baseline is used, the upper-bound VPL_e is lower than VAL throughout the entire service volume. In comparison, Fig. 8 shows that when the x_0 is increased to 1 km, the near-field VAL constraint dictates that a smaller p value (2×10^{-4}) is needed. This p value corresponds to a baseline length of approximately 500 m when $\sigma_{\Delta\phi} = 1$ cm. Note that, in this case, considerable margin exists in the far field.

A general observation that can be made from Figs. 7 and 8 is that, for small x_0, far-field VAL constraints define the required value of p, whereas when x_0 is large, the near-field VAL boundary is more

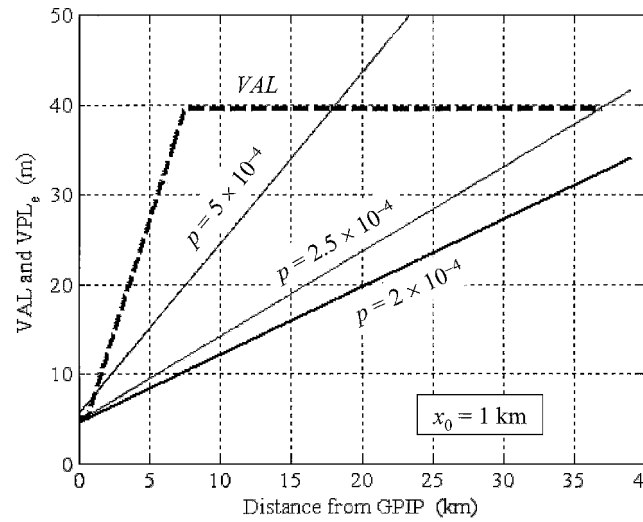

Fig. 8 VPL_e bound vs distance, $x_0 = 1$ km.

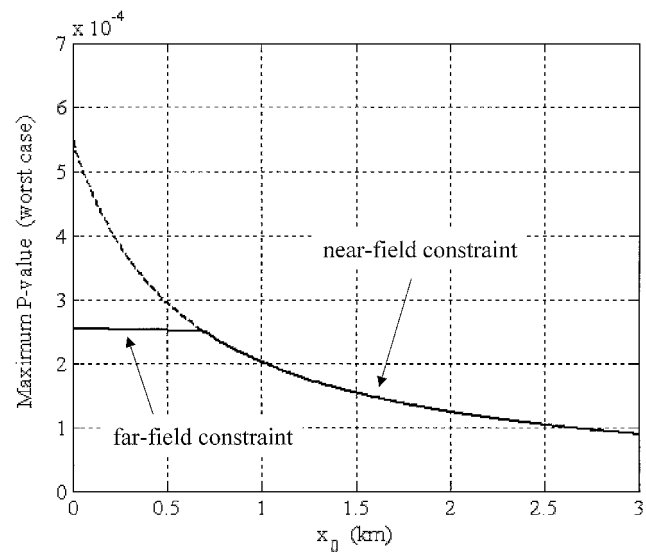

Fig. 9 Required P value vs x_0.

constraining. This is demonstrated quantitatively in Fig. 9, which is a plot of maximum permissible p value as a function of x_0. It is clear from Fig. 9 that, for a value of x_0 of approximately 0.7 km, near-field and far-field VAL constraints are of equal significance. Figure 10 is a representation of the same results as Fig. 9 in terms of minimum monitor baseline length. Note, however, that the baseline length requirements of Fig. 10 define the worst case in the sense that if the specified minimum baseline length is achievable, the ephemeris monitor will provide no availability penalty. If shorter baseline lengths are used, integrity will still be ensured because the broadcast p value (used by the aircraft to compute VPL) will be correspondingly larger. However, in this case, it is occasionally possible that $VPL_{H0} < VAL$ when $VPL_e > VAL$, resulting in an availability penalty due solely to the limited detection capability of the monitor. Because the availability requirements for LAAS are variable, the resulting tradeoff between acceptable LAAS navigation availability and required reference receiver baseline length can be optimized on an airport-by-airport basis.

In this analysis, we have assumed a single baseline aligned with an approach path situated in the local horizontal plane. When two orthogonal, horizontal reference receiver baselines are used, the relative runway orientation is irrelevant. Nevertheless, it is clear from Fig. 3 that the aircraft approach path does not actually lie in the horizontal plane, but is in fact vertically displaced by a 3-deg glide path angle. Because of its vertical displacement, the aircraft can potentially be affected by ephemeris errors that cannot be observed

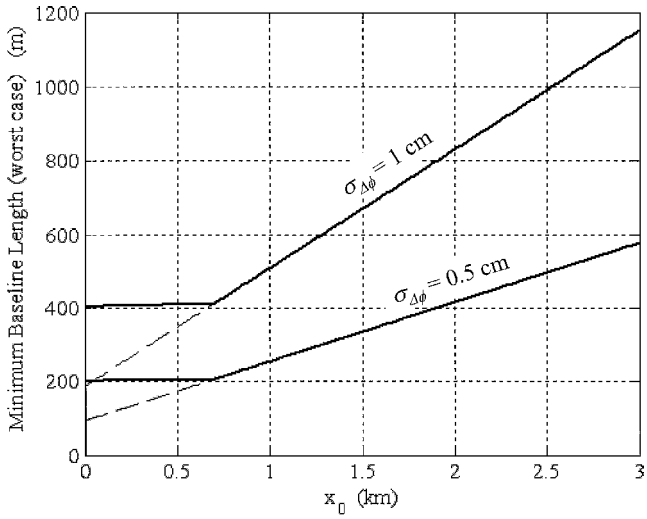

Fig. 10 Required baseline length vs x_0.

by horizontal baselines on the ground. [Using Eq. (7), one can always find an orbit error vector $\delta \boldsymbol{R}_i$ that is sensitive to vertical displacements only.] Therefore, to detect such ephemeris errors on the ground, a single additional reference baseline with a vertical displacement must be introduced. The necessary vertical displacement is easily obtained by scaling the required horizontal baseline length for $x_0 = 0$ in Fig. 10 by a factor of tan(3 deg). (Use of $x_0 = 0$ is appropriate here because the fixed vertical deviation between the GPIP and the reference receiver antenna centroid will be relatively small.) The resulting vertical baseline displacement required is approximately 10 m for $\sigma_{\Delta\phi} = 0.5$ cm and 20 m for $\sigma_{\Delta\phi} = 1$ cm.

Cycle Ambiguity Resolution

To initialize the carrier-phase ephemeris monitor for rising satellites, the integer-cycle ambiguities must be correctly resolved. There are a number of different algorithms available for this purpose. We choose a geometry-free widelane method[13] because it is an approach that does not implicitly assume that the broadcast ephemeris is correct.

Geometry-Free Widelane Method

Fundamental to the widelane method are the facts that the carrier-cycle ambiguity is an integer and that the difference between carrier and code measurements provides a direct (but noisy) observation of the cycle ambiguity. If the code measurement error could be reduced to one-half of the carrier wavelength (or less), the integer solution could be obtained directly by rounding. Unfortunately the L1 and L2 carriers have very short wavelengths; thus, reducing the noise floor of code measurements to one-half wavelength is not possible. However, it is possible to make the effective carrier wavelength longer by using the L1 and L2 carriers to construct a widelane (beat-frequency) signal Lw. Using Eq. (3), we define single difference carrier-phase measurements for two satellites, i and j:

$$\lambda_1 \Delta\phi_{ab}^{i} = \Delta r_{ab}^{i} + c(\delta t_b - \delta t_a) + \lambda_1 \Delta N_{ab}^{i} + \Delta\nu_{\phi}^{i}$$

$$\lambda_1 \Delta\phi_{ab}^{j} = \Delta r_{ab}^{j} + c(\delta t_b - \delta t_a) + \lambda_1 \Delta N_{ab}^{j} + \Delta\nu_{\phi}^{j}$$

A double-difference equation can be obtained by subtracting the second equation from the first:

$$\Delta^2\phi_{ab}^{ij} = (1/\lambda_1)\Delta^2 r_{ab}^{ij} + \Delta^2 N_{ab}^{ij} + (1/\lambda_1)\Delta^2\nu_{\phi}^{ij} \tag{30}$$

In this section, the superscripts i, j and the subscripts a, b will be dropped to simplify notation. However, another subscript, 1 or 2, is added to indicate carrier frequency L1 and L2, respectively.

When the double-difference carrier-phase measurement Eq. (30) is rewritten for L1 and L2 bands using simplified notation,

$$\phi_1 = (1/\lambda_1)r + N_1 + (1/\lambda_1)\tilde{\nu}_{\phi 1} \tag{31}$$

$$\phi_2 = (1/\lambda_2)r + N_2 + (1/\lambda_2)\tilde{\nu}_{\phi 2} \tag{32}$$

where $\sigma(\tilde{\nu}_{\phi 2}) \approx \sigma(\tilde{\nu}_{\phi 1}) = 2\sigma(\nu_\phi)$, and $\sigma(\nu_\phi)$ is the standard deviation of the raw carrier (L1 or L2) measurement error.

The widelane measurement is constructed by subtracting Eq. (32) from Eq. (31):

$$\phi_w \equiv \phi_1 - \phi_2 = r(1/\lambda_w) + N_w + (1/\lambda_w)\nu_{\phi w} \tag{33}$$

where $\sigma(\nu_{\phi w}) = 2\sqrt{2}\sigma(\nu_\phi)$ and the wavelength of the widelane signal is

$$\lambda_w = 1/(1/\lambda_1 - 1/\lambda_2) = 86.2 \text{ cm}$$

which is about 4.5 times longer than the L1 carrier wavelength.

One can also construct a double-difference L1 code measurement in the same way:

$$\rho = r + \tilde{\nu}_\rho \tag{34}$$

where $\sigma(\tilde{\nu}_\rho) = 2\sigma(\nu_\rho)$. Note that, although the L2 code measurement is not available for civil use, it is not needed for our purposes here. We combine code measurement (34) and widelane carrier measurement (33) to estimate the widelane integer N_w,

$$\hat{N}_w = \phi_w - \rho/\lambda_w \tag{35}$$

The error on the widelane integer estimate has variance:

$$\sigma^2(\hat{N}_w) = \left(1/\lambda_w^2\right)\left[\sigma^2(\tilde{\nu}_\rho) + \sigma^2(\nu_{\phi w})\right]$$

$$= \left(4/\lambda_w^2\right)\left[\sigma^2(\nu_\rho) + 2\sigma^2(\nu_\phi)\right] \tag{36}$$

Assuming for the moment that we obtain the correct integer via $N_w = \text{round}(\hat{N}_w)$, we can then estimate N_1 ($\Delta^2 N_{ab}^{ij}$ for L1) by solving the following equations:

$$\left.\begin{aligned} N_1 - N_2 &= N_w \\ N_1 - (\lambda_2/\lambda_1)N_2 &= \phi_1 - (\lambda_2/\lambda_1)\phi_2 + \tilde{\nu}_{\phi 12} \end{aligned}\right\} \Rightarrow \hat{N}_1$$

$$= (\lambda_2/\lambda_1 - 1)^{-1}\{(\lambda_2/\lambda_1)N_w - [\phi_1 - (\lambda_2/\lambda_1)\phi_2]\} \tag{37}$$

where

$$\sigma(\tilde{\nu}_{\phi 12}) = (1/\lambda_1)\left[4\sigma^2(\nu_{\phi 1}) + 4\left(\lambda_2^2/\lambda_1^2\right)\sigma^2(\nu_{\phi 1})\right]^{\frac{1}{2}}$$

$$= \left(\sqrt{10.59}/\lambda_1\right)\sigma(\nu_\phi)$$

and the standard deviation of the L1 integer estimate error is

$$\sigma(\hat{N}_1) = (\lambda_2/\lambda_1 - 1)^{-1}\left(\sqrt{10.59}/\lambda_1\right)\sigma(\nu_\phi) \approx (11.5/\lambda_1)\sigma(\nu_\phi) \tag{38}$$

Now, we turn attention to determining the probabilities that round $(\hat{N}_w)$ and round$(\hat{N}_1)$ yield the correct integers N_w and N_1, respectively. The probability of error in computing N_w is dependent on the size of $\sigma(\hat{N}_w)$. If $\sigma(\hat{N}_w)$ can be reduced, one can expect a higher probability that round$(\hat{N}_w) = N_w$. To meet a particular probability requirement for incorrect resolution, the average of a sequence of independent $\hat{N}_w$ estimates can be taken over a finite time period to reduce $\sigma(\hat{N}_w)$. However, the averaging time must be reasonably short (a few minutes at most) because a newly rising satellite cannot be approved for use by the aircraft until the monitor is initialized. For a given averaging time in which n_w independent estimates of $\hat{N}_w$ are available, the estimate error standard deviation of the averaged $\hat{N}_w$ is

$$\sigma_{w/\text{av}} = \sigma(\hat{N}_w)/\sqrt{n_w} \tag{39}$$

Assume now a minimum probability requirement $P(C_{Nw})$ for the correct resolution of N_w. Given $\sigma_{w/\text{av}}$, Eq. (40) must be satisfied to get an acceptable integer solution:

$$K_w \sigma_{w/\text{av}} \leq \tfrac{1}{2} \text{ cycle} \tag{40}$$

where K_w is a multiplier corresponding to the probability $P(C_{Nw})$, assuming a standard normal distribution. The same procedure is

applicable to cycle ambiguity N_1 with a probability requirement $P(C_{N1})$, or, equivalently, probability multiplier K_1:

$$K_1\sigma_{1/\text{av}} \le \tfrac{1}{2}\text{ cycle} \tag{41}$$

where

$$\sigma_{1/\text{av}} = \sigma(\hat{N}_1)\Big/\sqrt{n_1} \tag{42}$$

and n_1 is the total number of independent $\hat{N}_1$ estimates obtained during the averaging interval.

To proceed further, the probability requirements for correct integer resolution $\hat{N}_w$ and $\hat{N}_1$ must be quantified. These requirements can be derived from the specifications of category 3 LAAS.

Probability Allocations for Cycle Resolution

To allocate probability requirements for cycle resolution, it is necessary to understand in more detail how the system will detect satellite ephemeris errors. When it is assumed that an ephemeris error exists on satellite j and that $\Delta^2 N_{ab}^{ij}$ (same as N_1 in the simplified notation) has been correctly resolved using the technique described, a double difference L1-carrier residual can be formed using Eqs. (4) and (30) as follows:

$$\Delta^2\phi_{ab}^{ij} - (1/\lambda)\left[e_i^T - e_j^T\right]x_{ab} - \Delta^2 N_{ab}^{ij} = \delta e_j^T x_{ab} + \Delta^2 v_\phi \tag{43}$$

where all quantities on the left-hand side are known.

In general, when an ephemeris error exists, the magnitude of the residual, $|\delta e_j^T x_{ab} + \Delta^2 v_\phi|$, will be larger than the nominal value due to measurement noise alone, $|\Delta^2 v_\phi|$. Therefore, a threshold can be set using the residual as a test statistic to detect ephemeris error. When the residual exceeds the threshold, the system will trigger an alarm to warn the users to exclude the dangerous satellite. In this context, there exist two possible situations under which an alarm can be generated: 1) a valid alarm, which is caused by the existence of an actual ephemeris anomaly, and 2) a false alarm (FA), which can result either from an incorrect resolution of the integer or large measurement error due to nominal sources (such as multipath).

Ideally, we want to set a threshold that is high enough to minimize FAs but also low enough to provide acceptable ephemeris error detection performance. The probability P of ephemeris monitor false alarm can be expressed as follows:

$$P(\text{FA}) = P(\text{FA}|N_1\text{ wrong})P(N_1\text{ wrong}) + P(\text{FA}|N_1\text{ correct})P(N_1\text{ correct}) \tag{44}$$

To obtain an upper bound on $P(\text{FA})$, we assume $P(N_1$ correct$)=P(\text{FA}\ |N_1$ wrong$)=1$. The resulting bound is tight because any operationally useful system must ensure that $P(N_1$ wrong$)$ is very small, and given that N_1 is wrong, the residual would exceed any reasonable threshold almost instantly. Under these conservative assumptions, the FA probability (upper bound) can be simplified as

$$P(\text{FA}) = P(N_1\text{ wrong}) + P(\text{FA}|N_1\text{ correct}) \tag{45}$$

A rising satellite will be declared unavailable for use by the LAAS reference station if the residual test fails immediately following cycle resolution. Because there is some flexibility with regard to availability of any particular LAAS implementation (as noted earlier), we assume a reasonably conservative requirement consistent with LAAS system availability guidelines in Ref. 9:

$$P(\text{satellite unavailable}) = P(N_1\text{ wrong}) + P(\text{FA}|N_1\text{ correct}) \le 10^{-4} \tag{46}$$

However, the residual test is executed throughout a satellite pass (after initial approval of the satellite), so that $P(\text{FA}\ |N_1$ correct$)$ is also constrained by continuity requirements. This is true because once a satellite was declared as available by the system, a subsequent FA will terminate usage of the satellite and risk loss of continuity. Therefore, $P(\text{FA}\ |N_1$ correct$)$ must be consistent with a suballocated FA requirement derived from the category 3 LAAS continuity risk specification (1×10^{-7}):

$$P(\text{FA}|N_1\text{ correct}) \le 10^{-7} \tag{47}$$

Recall that the probability multiplier $K_{\text{ffde}}=5.3$ (used earlier to define detection threshold T_s) is consistent with this requirement.

Noting that $P(\text{FA}\ |N_1$ correct$)\ll10^{-4}$, we can now simplify the availability constraint in Eq. (46):

$$P(N_1\text{wrong}) \le 10^{-4} \tag{48}$$

In turn, the probability of incorrect integer resolution can be divided into two parts, consistent with the widelane procedure:

$$P(N_1\text{ wrong}) = P(N_1\text{ wrong}|N_w\text{ wrong})P(N_w\text{ wrong}) + P(N_1\text{ wrong}|N_w\text{ correct})P(N_w\text{ correct}) \tag{49}$$

To obtain an upper bound for $P(N_1$ wrong$)$, we conservatively assume $P(N_1$ wrong $|N_w$ wrong$)$ and $P(N_w$ correct$)$ are unity:

$$P(N_1\text{ wrong}) \le P(N_w\text{ wrong}) + P(N_1\text{ wrong}|N_w\text{ correct}) \tag{50}$$

Note that inequality (50) represents a tight bound because, for an operationally viable monitor, the probabilities of incorrect integer resolution must be very small.

For simplicity we can choose to allocate the $P(N_1$ wrong$)$ constraint from Eq. (48) evenly as follows:

$$P(N_w\text{ wrong}) = P(N_1\text{ wrong}|N_w\text{ correct}) = 5\times10^{-5} \tag{51}$$

In this case, $K_w=K_1=4.06$. We now turn our attention to defining the maximum acceptable standard deviations of pseudorange and carrier-phase measurements consistent with operationally acceptable initialization (averaging) times.

Ranging Measurement Error Requirements

The number of independent measurement samples (or, equivalently, the duration of the initial time interval) required to estimate N_w and N_1 with the required probabilities of success can now be defined. For the widelane integer, solving for n_w using relations (39) and (40) and noting that $\sigma(\nu_\phi)\ll\sigma(\nu_\rho)$, we have

$$n_w \ge [16.24\times\sigma(\nu_\rho)/\lambda_w]^2 \tag{52}$$

Likewise for the L1 integer, using Eqs. (41) and (42), we obtain

$$n_1 \ge [93.38\times\sigma(\nu_\phi)/\lambda_1]^2 \tag{53}$$

The minimum number of independent samples n_w and n_1 are clearly functions of the range measurement error standard deviations which, in turn, are functions of GPS antenna quality. For example, using ranging error data for rising satellites collected with nominal performance antennas (NovAtel Choke Ring Model 503) mounted in a relatively high-multipath environment on a rooftop at the Illinois Institute of Technology (IIT), $\sigma(\nu_\rho)\approx0.6$ m and $\sigma(\nu_\phi)\approx0.01$ m. Substituting these numbers into Eqs. (52) and (53), we have $n_w\ge128$ and $n_1\ge24$. Clearly, widelane integer N_w estimation is the primary driver for initialization time because the minimum number of independent measurements to estimate N_w is much larger than the number of samples to estimate N_1. (Once N_w is determined, an ample number of measurements to estimate N_1 is also available. Thus, integer N_1 can be resolved instantly.)

The LGF will employ state-of-the-art multipath limiting antennas (MLAs), which have been demonstrated to provide ranging error performance that is superior to that of nominal GPS antennas.[14] An example raw pseudorange error data using an MLA is shown in Fig. 11. These data were collected at the LAAS test prototype facility at the William J. Hughes FAA Technical Center in Atlantic City, New Jersey. The standard deviation of the error data is 16 cm, which yields $n_w\ge9$ using Eq. (52), a dramatic reduction in initialization time relative to the choke ring antenna. Furthermore, the correlation time of the raw pseudorange error is approximately 10 s, which suggests a required initialization time of less than 5-min duration is achievable. Nevertheless, additional field testing with dual frequency MLA antennas (currently under development) will be needed to verify that such short initialization times are consistently realizable in airport multipath environments.

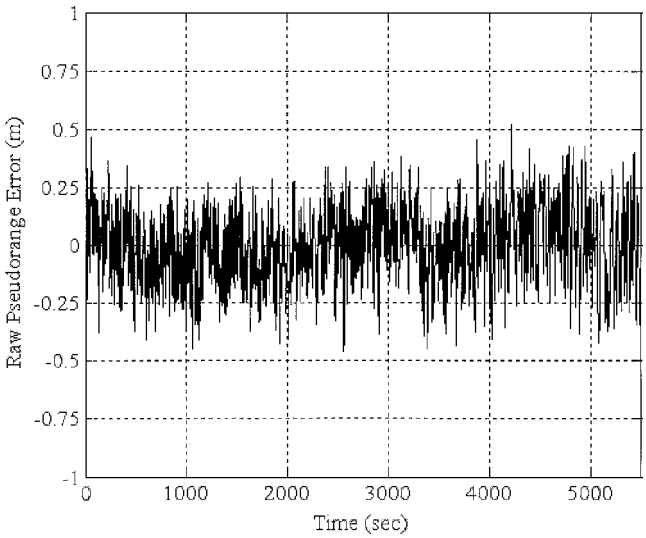

Fig. 11 Example MLA raw pseudorange error data.

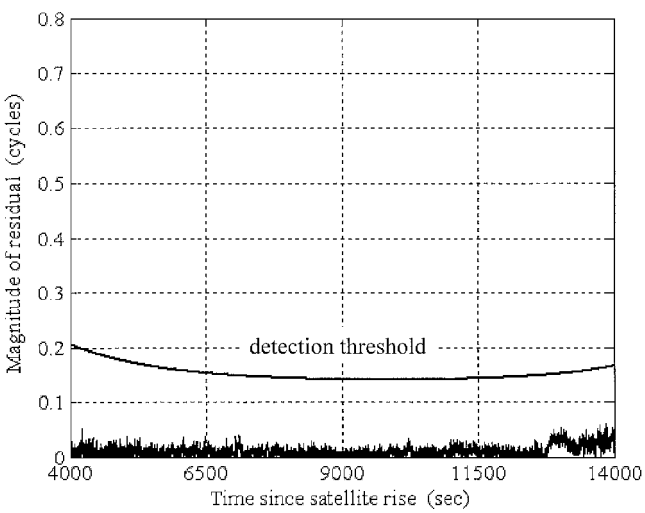

Fig. 12 Residuals of double-difference carrier-phase measurements.

Experimental Example

To demonstrate the ability of the monitor to detect orbit ephemeris errors, L1 and L2 carrier-phase measurements and L1 code measurements were collected from two receivers in March 2001. The receivers used were NovAtel Millennium GPSCard connected to L1/L2 GPS Choke Ring Antennas (Model 503). The antennas were located on the rooftop of the Engineering 1 building at IIT and were separated by a baseline of approximately 26 m. Because the antennas are not MLA type and the available baseline was short relative to what can be realized at an airport, the intent of this experiment was not to demonstrate a level of availability performance (initialization time and p value) applicable to LAAS. Instead, the purpose of the experiment was to show that the monitor concept is realizable with existing technology.

Carrier-phase data for two satellites (one rising) were processed via double differencing in two stages. First, the cycle ambiguity N_w was resolved by averaging 120 independent samples taken over the duration of the rising satellite pass. Subsequently, N_1 was resolved instantly. In the second stage, the resolved cycle ambiguity N_1 was removed from the double-difference measurements to generate the residual for fault detection. An ephemeris error was later deliberately injected into the data.

Figure 12 shows the double-difference carrier residual history for an example satellite without ephemeris error. The higher noise magnitude during the periods at the beginning and end of the residual history correspond to low-elevation angles for the satellite. This behavior is typical for the NovAtel antenna because the effect of multipath is more significant at low elevations. Therefore, the standard deviation of carrier measurement error is larger at low elevation angles, and the resulting threshold is also correspondingly larger via Eq. (18).

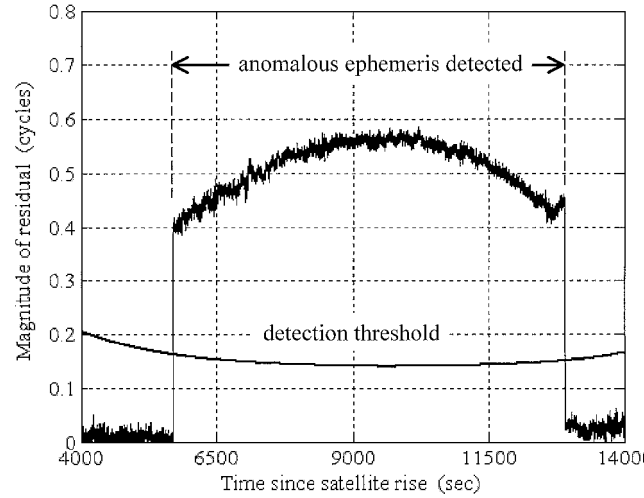

Fig. 13 Carrier residuals with ephemeris error injection.

In contrast, Fig. 13 shows the residual history for the same satellite when an ephemeris error is deliberately injected during the satellite pass. Here, the eccentricity of the orbit was changed by adding 0.003 to the nominal value. The erroneous eccentricity was maintained for 2 h to simulate the duration of the actual broadcast ephemeris update period used by the GPS satellites. The response of the residual to the injected parameter error is immediate, and the elevated level is sustained for the duration of the ephemeris anomaly.

Conclusions

The DGPS concept has demonstrated great improvements in position accuracy relative to stand-alone GPS usage. The technique has been used widely in various applications, including the FAA's LAAS for aircraft precision approach and landing. Because knowledge of correct satellite orbit data is fundamental to differential positioning, ephemeris monitoring is necessary to ensure navigation integrity.

We described a new method to detect orbit errors affecting DGPS users based on carrier-phase measurements made by two or more ground-based reference receivers separated by short baselines. A dual-frequency, geometry-free widelane approach is used to resolve the unknown cycle ambiguities in the carrier-phase measurements. The proposed integrity monitor provides real-time detection capability for orbit ephemeris anomalies following scheduled or unscheduled spacecraft maneuvers (type A) and general errors in the broadcast ephemeris data not attributable to spacecraft maneuvers (type B).

Acknowledgments

The authors gratefully acknowledge the Federal Aviation Administration for supporting this research. The constructive comments and advice regarding this work provided by Samuel P. Pullen are greatly appreciated.

References

[1] "Specification: Category One Local Area Augmentation System Non-Federal Ground Facility," Federal Aviation Administration, FAA/AND710-2937, U.S. Department of Transportation, May 2001.

[2] Parkinson, B., and Axelrad, P., "Autonomous Integrity Monitoring Using the Pseudorange Residual," *Navigation*, Vol. 35, No. 2, 1988, pp. 255–274.

[3] Sturza, M., "Navigation System Integrity Monitoring Using Redundant Measurements," *Navigation*, Vol. 35, No. 4, 1988-1989, pp. 483–501.

[4] Brown, R., and McBurney, P., "Self-Contained GPS Integrity Check Using Maximum Solution Separation," *Navigation*, Vol. 35, No. 1, 1988, pp. 41–53.

[5] Matsumoto, S., Pullen, S., Rotkowitz, M., and Pervan, B., "GPS Ephemeris Verification for Local Area Augmentation System (LAAS) Ground Stations," *Proceedings of the 12th International Meeting of the Satellite Division of the Institute of Navigation*, Inst. of Navigation, Alexandria, VA, 1999, pp. 691–704.

[6]Chan, F.-C., "Detection of Global Positioning Satellite Orbit Errors Using Short-Baseline Carrier Phase Measurements," M.S. Thesis, Dept. of Mechanical, Materials, and Aerospace Engineering, Illinois Inst. of Technology, Chicago, Aug. 2001, pp. 17–19.

[7]Davis, J., and Kelly, R., "RNP Tunnel Concept for Precision Approach with GNSS Application," *Proceedings of Institute of Navigation 49th Annual Meeting*, Inst. of Navigation, Alexandria, VA, 1993, pp. 135–154.

[8]"Operational Requirements Document: Local Area Augmentation System," Satellite Navigation Program Office, Federal Aviation Administration, Washington, DC, Feb. 1995.

[9]"Minimum Aviation System Performance Standards for the Local Area Augmentation System," RTCA, Inc., Rept. SC-159 WG-4A, DO-245, Washington, DC, Sept. 1998, pp. 12, 19, 34.

[10]Jefferson, D., and Bar-Sever, Y., "Accuracy and Consistency of Broadcast GPS Ephemeris Data," *Proceedings of the 13th International Technical Meeting of the Satellite Division of the Institute of Navigation*, Inst. of Navigation, Alexandria, VA, 2000, pp. 391–395.

[11]"Minimum Operational Performance Standards for GPS Local Area Augmentation System Airborne Equipment," RTCA, Inc., Rept. SC-159 WG-4A, DO-253, Washington, DC, Jan. 2000.

[12]Shively, C. A., "Preliminary Analysis of Requirements for Cat IIIB LAAS," *Proceedings of the 57th Annual Meeting of the Institute of Navigation*, Inst. of Navigation, Alexandria, VA, 2001, pp. 705–714.

[13]Misra, P., and Enge, P., *Global Positioning System: Signals, Measurements, and Performance*, Ganga-Jamuna, Lincoln, MA, 2001, pp. 230–233.

[14]Warburton, J., and Lamb, D., "Validation of the FAA LAAS Specification Using the LAAS Test Prototype (LTP)," *Navigation*, Vol. 45, No. 4, 1998-1999, pp. 265–274.